TESTING THE RELATIONSHIP BETWEEN SATURN'S ENA AND NARROWBAND RADIO EMISSIONS

Joe Kinrade[1], Sarah V. Badman[1], Chris Paranicas[2], Caitriona M. Jackman[3], Corentin K. Louis[3], and Elizabeth O'Dwyer[3].

Abstract

Saturn's kilometric radiation (SKR) and Energetic Neutral Atom (ENA) emissions are important remote diagnostics of the planet's magnetospheric dynamics, intensifying during periods of global-scale plasma injection, and displaying characteristic planetary periodicity. Global-scale ENA signatures have been associated with narrowband radio emissions around 5 and 20 kHz, particularly at evening local times where plasma injections are expected to have moved inwards through the magnetosphere, triggering interchange instabilities. Narrowband radio emission sources are associated with density gradients at the inner edges of the Enceladus plasma torus that promote wave mode conversion, but any radial distance dependence with the ENA emission is untested. We constrain ENA keograms to distances covering the 'inner' and 'outer' magnetosphere separately, and quantify the correlation between the ENA intensity with narrowband flux density in the 5 and 20 kHz emission bands. One case study shows a spiral ENA morphology that indicates global-scale plasma injection activity. 'Bursts' of narrowband emission coincide with the rotation of ENA enhancements through the dusk-midnight local time sector in the inner magnetosphere, but at earlier times in the outer magnetosphere, consistent with inward flow of the injected plasma as it drifts around the planet. A second case study with similar observing conditions shows clear 5 kHz radio bursts, but very low levels of ENA detections, indicating that the relationship is not always so general in these data. These results contribute towards our developing picture of how global plasma injection events can influence Saturn's inner magnetosphere, linking together two valuable sources of remotely sensed global emissions, the ENAs and narrowband radio emissions.

[1]*Lancaster University, UK*
[2]*JHU APL, Maryland, USA*
[3]*DIAS, Dublin, Ireland*

1 Introduction

Saturn's narrowband NB radio emissions were first discovered during the Voyager mission (Gurnett et al., 1981). They are distinct from the 'mainband' kilometric radiation (SKR) because they have a different formation mechanism; SKR is generated by the Cyclotron Maser Instability (CMI), and beamed such that there is a clear local-time restricted pattern for the strongest emission, and a relationship to the intensity of energetic particle precipitation into the auroral zones (Lamy et al., 2008, 2009; Lamy, 2017). Narrowband emissions are driven differently (via mode conversion) and much remains to be understood about their link to SKR and to global magnetospheric dynamics.

The sources of Saturn's narrowband emissions are thought to be in regions of plasma density gradients at the inner edges of the Enceladus plasma torus (L shells of between 4-10) via mode conversion of electrostatic waves (e.g., Gurnett et al., 1981; Menietti et al., 2009; Ye et al., 2009, 2011). Two distinct bands of narrowband emission exist around 5 and 20 kHz, typically detected after intensification of the main-band SKR (100-400 kHz), persisting for up to several days (Wang et al., 2010). Although separate terms exist in the literature for the 5 kHz band (n-SMR, Louarn et al., 2007) and 20 kHz band (n-SKR, Lamy et al., 2008), we refer to them collectively here as narrowband or 'NB.'

Saturn's neutral-dominated magnetosphere is an efficient emitter of energetic neutral atoms (ENAs), created mainly through charge exchange of energetic ions with the extended neutral cloud originating from the icy moon Enceladus. Throughout the Cassini mission, its Ion Neutral Camera (INCA) (Krimigis et al., 2004) has helped to reveal the global plasma dynamics throughout Saturn's magnetosphere, providing wide-angle images of this magnetospheric ENA emission. The most distinctive features of ENA imagery from Saturn are signatures of global-scale plasma injection following reconnection activity in the magnetotail. Distinct regions of enhanced ENA emission appear in the midnight-dawn local time sector at distances of at least $\sim$20 R_S (e.g., Hill et al., 2008), and then rotate inwards and around the planet at a bulk speed of $\sim$60-70% rigid corotation Carbary & Mitchell (2014). These can persist for several days before dissipating (Paranicas et al., 2005), and have been observed to periodically 're-energize' in the midnight sector (Mitchell et al., 2009). Statistically the ENA emission is modulated by Saturn's ubiquitous planetary-period oscillations (PPOs) (Carbary et al., 2008a; Kinrade et al., 2021), possibly due to plasmasheet thickness variations, and they often have counterpart signatures in the ultraviolet auroras Mitchell et al. (2009); Kinrade et al. (2020).

A close correspondence has been observed between 'bursts' of NB emission and rotating regions of enhanced ENA intensity in the magnetosphere, particularly as they pass through the dusk-midnight local time sector (Wang et al., 2010; Mitchell et al., 2015). The fact that both the NB and ENA emissions are modulated at near the planetary period ($\sim$10.5 h) (e.g., Paranicas et al., 2005; Ye et al., 2010; Wing et al., 2020; Kinrade et al., 2021) tells us that this correspondence is likely linked with the periodic injection of hot plasma into the inner magnetosphere following reconnection events in the magnetotail (e.g., Bradley et al., 2018). It is a complex picture at Saturn, a cascade of large-to-small scale plasma transport and instability triggering, around the planet and inwards through the magnetosphere. It's important to note that ENA production is a function of neutral density as well as ion density, both of which vary across the radial distances of interest here (e.g., Thomsen et al., 2010; Smith & Richardson, 2021). An outstanding question is how does injected plasma cause a response in radio emissions? Can we use the ENA emission to locate local time sectors and/or radial distances likely to have plasma density gradients that promote the production of NB emissions?

Detection of the free space ordinary mode (L-O) NB by Cassini is typically only possible from highly inclined orbit positions, since the emissions - with more intense Z-mode sources deep in the magnetosphere (Menietti et al., 2016) - are blocked or reflected by density gradients at the inner-edge of the plasma torus, when they mode convert to the weaker L-O mode more readily detected by Cassini at greater distances in the magnetosphere (Ye et al., 2009; Wu et al., 2022a). Both left-handed (LH) and right-handed (RH) circular polarization modes of the NB can be observed in either hemisphere, particularly at high latitudes (e.g., Ye et al., 2010). Note that at distances beyond 10 R_S Note the circular polarization sense is opposite to that of the mainband SKR (100-400 kHz), with LH (RH) NB emitted mainly in the north (south) hemisphere (Ye et al., 2011). Wu et al. (2021) surveyed RPWS measurements for NB detection and observed a peak intensity of the 5 kHz and 20 kHz emissions at a spacecraft distance of $\sim$6 R_S, with the 5 kHz also showing a higher occurrence in the dusk sector. This is close to the average inner boundary of the ENA emission intensity at 7-10 R_S based on the mission average images of Kinrade et al. (2021), and thus where we expect temperature anisotropies and density gradients associated with plasma transport following global injection events. Surveys of interchange-driven injection signatures in energetic H+ particles also show a dusk-night side preference at similar inner magnetosphere distances 7-9 R_S (e.g., Azari et al., 2018).

Wing et al. (2020) demonstrated a detailed time-lag analysis of Saturn's ENA and NB emissions based on eight case-study events, finding that the innermost ENA injection signatures (i.e., close to the planet, or 'Type 2') correlate best with the 5 kHz radio emission, lagging the ENA injection by a few minutes up to several hours. They used ENA intensity in the radial distance range to 5-9 R_S in the equatorial plane, and tested local times between 21-03 LT. Here we consider the ENA emission across a range of radial distances, and at all local times, therefore capturing the full rotation pattern of ENA enhancements and building on the work of Wing et al.. Section 2 briefly introduces the radio and ENA data, and Section 3 presents two case studies that demonstrate the cross-correlation analysis. Section 4 is a brief discussion and summary.

2 Data

2.1 ENA Imagery from the Cassini INCA

We use equatorial projections of the Magnetospheric Imaging Instrument (MIMI) /INCA imagery (Krimigis et al., 2004), which have been cleaned, calibrated and re-sampled to a grid resolution of 1×1 R_S, using the processing steps described in Bader et al. (2021), including spacecraft motion compensation at every frame, sensor calibration, and removal of artefacts from sunlight and ion beams. Projections are shown in the Saturn-centred

Kronocentric Solar Magnetic (KSMAG) X-Y plane, where Z is directed along Saturn's dipole moment M, Y = $M \times S$ where S is the Saturn-Sun vector, and X is in the plane formed by the Saturn-Sun vector and Saturn's dipole moment, completing the right-hand set. At Saturn we may assume a spin-aligned dipole moment and so Z is along Saturn's spin axis and X-Y lies in Saturn's equatorial plane. We show images from the 24-55 keV H INCA energy band here, but images from the other INCA energy channels are also available in the projection dataset (see Acknowledgements). The ENA differential energy flux is in units of counts/cm^2-sr-s-keV. The INCA captured $\sim$4-minute integrations, and we average the intensities in the equatorial projections using a 60-minute time window (retaining a 4-minute resolution in the ENA keograms).

2.2 Kilometric Radio Spectra from Cassini RPWS

We use cleaned and resampled SKR flux densities, derived from the High Frequency Receiver (HFR) unit of Cassini's Radio and Plasma Waves Science (RPWS, Gurnett, 2004) instrument by Lamy et al. (2009). The full treatment of this data is detailed by Lamy et al. (2008), and the data are available on the LESIA/Kronos server (see Acknowledgements). To isolate the NB emissions in the spectrograms and extract a time series of emission power, we integrate the flux density across two bands encompassing the typical 5 kHz and 20 kHz frequencies; 3.55-7.64 kHz and 9.11-50.12 kHz respectively (spanning 20% bandwidth of the log-spaced central frequency bins as defined). The temporal resolution is 3 minutes. We've used polarized spectra here in order to help separate the NB emissions from the mainband SKR, dependent on hemisphere - particularly for the 20 kHz band which can be contaminated with low frequency extensions (LFEs) of the SKR. Another complication in isolating the NB emissions is the recently identified 'Saturn Anomalous Myriametric' (SAM) emission (Wu et al., 2022b) sitting partially in this frequency range (being centered around 13 kHz, with a bandwidth of 8 kHz), which tends to follow LFEs and is possibly linked with solar wind compressions.

3 Observations

We present two case studies, chosen because of data availability from both the INCA and the RPWS instruments, plus their similarity in observing geometry; Cassini's range and relatively high orbit inclination in each case allowing projection of the ENA imagery into the equatorial plane, and optimal viewing of the high-latitude NB emission.

3.1 Case study 1: 2007 DOY 096

On day 96 of 2007 (6 April), Cassini's inbound orbit was inclined by between $\sim$43-50° latitude at radial distances of 17-22 R_S above the northern hemisphere (1 R_S = 60,268 km), and simultaneous observations were taken by the INCA, UVIS and RPWS instruments. Figure 1 shows a series of equatorial projections (X-Y$_{KSMAG}$) of the ENA emission throughout 2007-096, window-averaged over $\sim$45-60 minutes. A spiral morphology is clearly observed in the magnetosphere . The ENA emission shows two clear rotations of a global-scale plasma injection throughout the day, with the injection covering >12 h LT over radial distances 5-20 R_S. The spiral morphology indicates the activation of plasma pressure gradient-driven transient current systems over a planetary rotation period (e.g., Mitchell et al., 2009; Kinrade et al., 2020; Palmaerts et al., 2020).Brandt et al. (2008) note that this spiral morphology does not always manifest in the ENA emission, and its presence indicates relatively stable drift patterns in the inner magnetosphere.

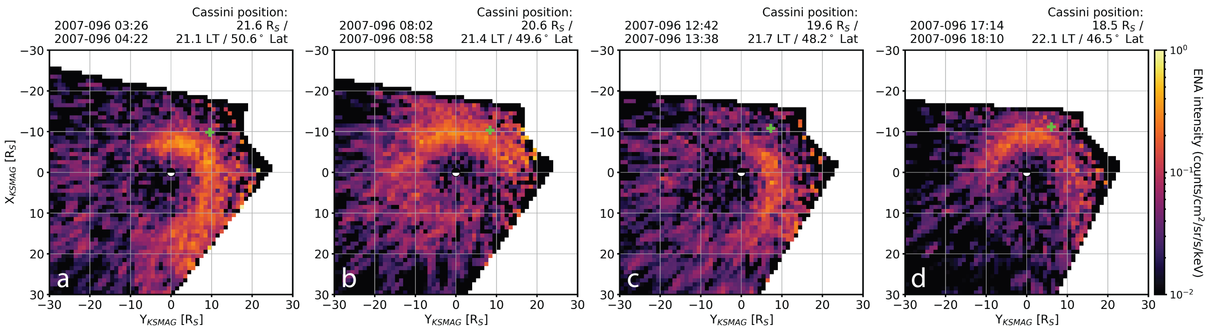

Figure 1: A series of images of the ENA emission captured by the Cassini INCA throughout 2007-096, projected into Saturn's equatorial KSMAG X-Y plane. Sun direction is towards the bottom of each image. A green cross shows Cassini's XY position at the centre of each ∼60-minute integration window, with position summary above. Saturn is shown in the centre of each image with day/night-side shading. Cassini's latitude was >43° throughout the day (north hemisphere), at a range of ∼19-22 R_S on the dusk side of the planet. Various stages of a spiral morphology are clear, with order-of-magnitude intensity changes visible within 10 R_S of the planet.

Figure 2a shows a frequency-time spectrogram of the narrowband radio data, which were dominated by LH-polarised emission during 2007-096. The horizontal dashed lines show the frequency ranges of interest for the 5 kHz and 20 kHz bands. Two intensifications or 'bursts' are visible in both bands at ∼04-08 UT and ∼14-18 UT (onsets labelled above Figure 2a). The NB flux density is highest in the 5 kHz band, but the 20 kHz does also show the same burst pattern, lasting over 3 hours in each case. The ENA morphology is strikingly similar during the times of these NB bursts, as shown in Figure 1. Figure 1a coincides with the first NB burst onset, showing the ENA spiral structure spanning local times covering noon (between radial distances ∼10-20 R_S), via dusk, around to post-midnight, being closest to the planet (∼5-10 R_S) - and brightest - around pre-midnight. By the time the first NB burst has faded in intensity ∼3-4 hours later, the ENA emission has rotated around the planet, encompassing local times between dusk to dawn via midnight, the leading edge of the spiral reaching dawn and possibly even noon considering lower intensities (Figure 1b). Similar ENA morphology is evident during the second NB burst, the enhanced emission region rotating around the planet a second time (Figures 1c,d). The onset of the radio bursts appears to be coincident with the leading edge of the ENA structure passing through the midnight local time sector.

Figure 2b shows a keogram of the ENA emission in a UT-LT frame. This keogram is constructed using the mean ENA emission intensity between 1-20 R_S (typically the useful extent of these INCA projections, out to Titan's orbit where the emission level drops

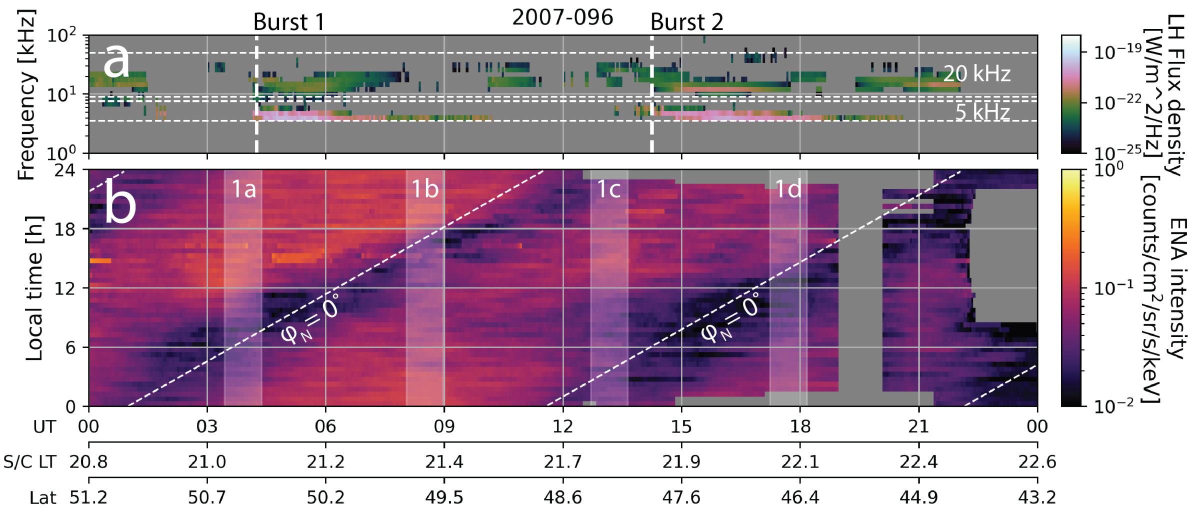

Figure 2: A comparison of Saturn's kilometric radio and ENA emissions during 2007-096. 2a (top) is a spectrogram showing the NB flux density for the left-hand (LH) polarization. Dashed horizontal lines show the two frequency bands used to integrate around the 5 and 20 kHz NB bands. Vertical lines in 2a mark the approximate start times of the two NB bursts, ten hours apart. 2b (bottom) is a keogram showing the mean ENA intensity between 1-20 R_S. Shaded time windows 1a-d show the extent of the four averaged INCA projections from Figure 1. Dashed diagonal lines indicate the local time direction of the rotating magnetic perturbation field dipole associated with Saturn's northern PPO system.

off significantly, plus the validity of the projection at acute angles). The rotating ENA enhancement imaged in Figure 1 is visible here as a series of diagonal bands, varying almost sinusoidally when considering a fixed point of local time as the plasma population drifts around the planet. Such keograms have been used to measure the drift speed of these ENA injection signatures (e.g., Carbary et al., 2008b; Kinrade et al., 2020), which typically drift at 60-70% rigid planetary co-rotation (although the effect of gradient-curvature drift spreads the hot plasma population azimuthally with time - see Mitchell et al. (2009)). For reference, the time extents of the projections in Figure 1 are shaded in Figure 2b. The keogram confirms that the first NB burst occurs when the leading edge of the ENA enhancement reaches midnight LT (compare Figures 2a,b, Figures 1a,b), and spans the entire dusk-side of the planet. Similar ENA morphology is apparent a rotation later with the onset of the second NB burst (compare a,b, Figures 1c,d). For reference, we have added the dipole phase of the northern magnetic planetary period oscillation (PPO) system (Provan, 2018) to the keogram as an indication of planetary rotation rate (since Cassini was in the northern hemisphere in this example).

We extract 'slices' through the ENA keogram at 48 local time bins (i.e., every 30 mins, or 7.5° azimuth around the planet), resulting in 48 separate time series showing how the mean ENA intensity varied with universal time at that local time sector. This is performed on two versions of the keogram, based on nominal distance ranges covering the 'outer magnetosphere' and 'inner magnetosphere'; 10-20 R_S and 5-10 R_S, respectively (obtained by cropping the ENA projections to these distance ranges). Figure 3a shows a time series of the NB emission power in the two frequency bands 3.55-7.64 and 9.11-50.12 kHz during

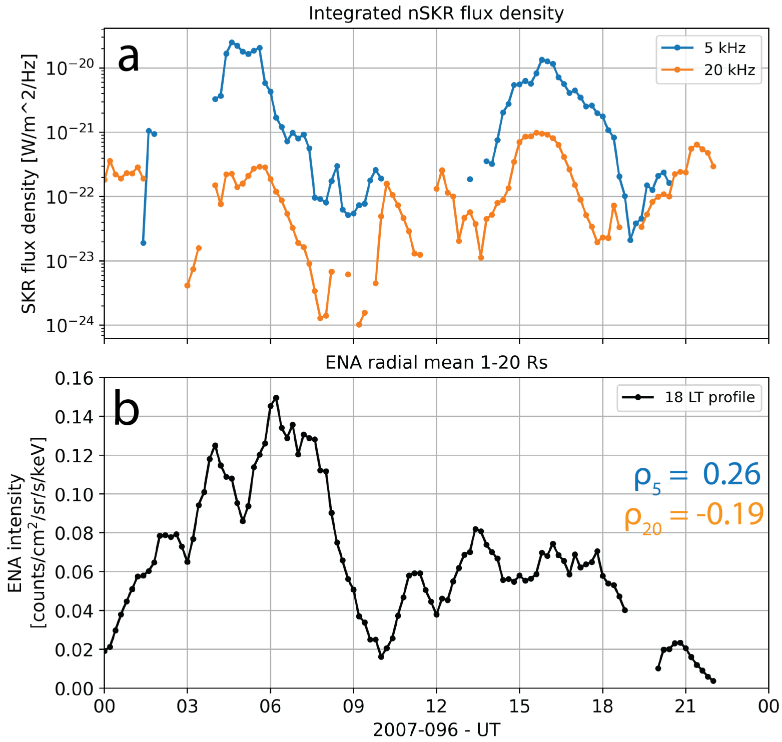

Figure 3: Time series during 2007-096 of (3a) NB emission power (integrated flux density) around the 5 and 20 kHz bands, and (3b) mean ENA emission intensity between 1-20 R_S at 18 LT. Each time series has been re-sampled to a 12-minute resolution. The respective linear cross-correlation values between the ENA and NB series are annotated in 3b.

day 2007-096. Figure 3b shows a time series of the mean ENA intensity in the radial range 1-20 R_S at 18 LT, as a dusk-sector example. A Pearson cross correlation ('x-c') value, ρ, is calculated for each of the two NB bands, correlated with the ENA LT profile across the full time window; in the case of Figure 3, $\rho = 0.26$ for the 5 kHz (slight correlation) and -0.19 (slight anti-correlation) for the 20 kHz (annotated in Figure 3b). We then calculate ρ for each of the 48 LT profiles of mean ENA intensity, thereby providing a global 'quick-look' comparison of where in LT the ENA and NB have the highest correlation. A Pearson x-c value of $\rho = 1$ means perfect correlation, -1 perfect anti-correlation. If the ENA intensity time series at a particular local time closely aligns with the NB power time series, the resulting correlation coefficient calculated for that time will approach 1. Conversely, an anti-correlation could indicate a local time delay between the two time series, especially since the ENA enhancement in this case is approximately sinusoidal in intensity around the planet for a fixed radial distance.

Figure 4 shows this summary view of the ENA-NB cross correlation at all local time bins, for inner (4a) and outer (4b) magnetosphere distances. In the outer (10-20 R_S) magnetosphere, the mean ENA intensity variations best match the 5 kHz NB emission profile around 15 LT (ρ ~0.75) and are slightly anti-correlated at dawn LTs (ρ ~-0.25). The 20 kHz x-c response shows a similar overall shape to the 5 kHz in LT, but is less pronounced and anti-correlated with ENA intensity at most LTs. At inner magnetosphere distances (5-10 R_S), the mean ENA intensity best matches the 5 kHz nSKR emission

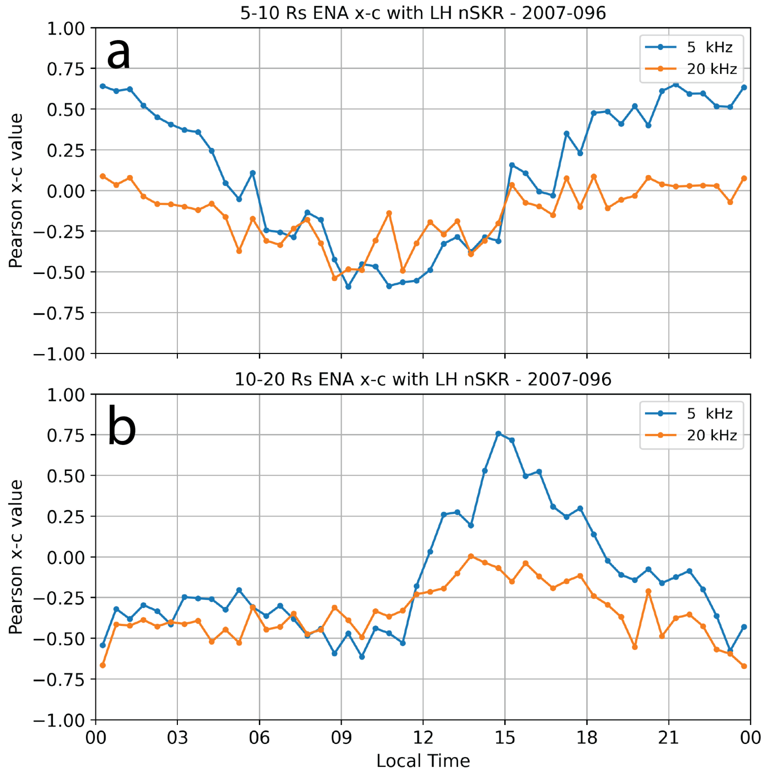

Figure 4: An overview of the cross-correlation between 48 ENA local time profiles and the integrated NB emission time series of Figure 3a, from day 2007-096. The 'inner magnetosphere' profiles (4a) are based on the ENA emission within the distance range 5-10 R_S, and the 'outer magnetosphere' profiles (4b) within 10-20 R_S. Comparison of 4a and 4b shows that the peak ENA-NB correlation shifts to later local times as the injected plasma population drifts inwards through the magnetosphere, likely a consequence of the spiral morphology of the plasma flow.

profile between ∼21-02 LT ($0.5 < \rho < 0.7$). This makes sense given the spiral morphology of the ENA emission, and the fact we expect plasma gradients to develop as the injected plasma population gradually drifts inwards and around the planet. The 20 kHz emission shows weak correlation with ENA intensity at the inner magnetosphere, but again shows a similar-shaped LT response to the 5 kHz. Figure 4 demonstrates an important ambiguity in the correlation exercise here - we do not know the exact local time or distance of the narrowband emission source, only a proxy for the general localized conditions that may lead to its production. It is not possible to distinguish precisely at which distances or local times the ENA emission appears to match best with the NB response, only that they change in an expected way depending on whether the comparison is made at outer or inner distances in the magnetosphere.

3.2 Case study 2: 2013 DOY 128

We have observed some cases where bursts of the narrowband radio emission exist in the absence of any clear ENA emission. Figure 5 shows an example from day 2013-128, when Cassini was at southern high-latitudes, post-noon LTs, at distances of 21.6-18.3 R_S.

There are two bursts of NB visible in the 5 kHz band at ∼06-10 UT and ∼16-21 UT at similar intensities to the previous example, but in RH polarization here since Cassini was in the Southern hemisphere. Emission around the 20 kHz band is also detected but with less clearly defined bursts. The ENA keogram, however, shows very weak emission below the intensities observed in the previous example (comparing Figures 2 and 5).

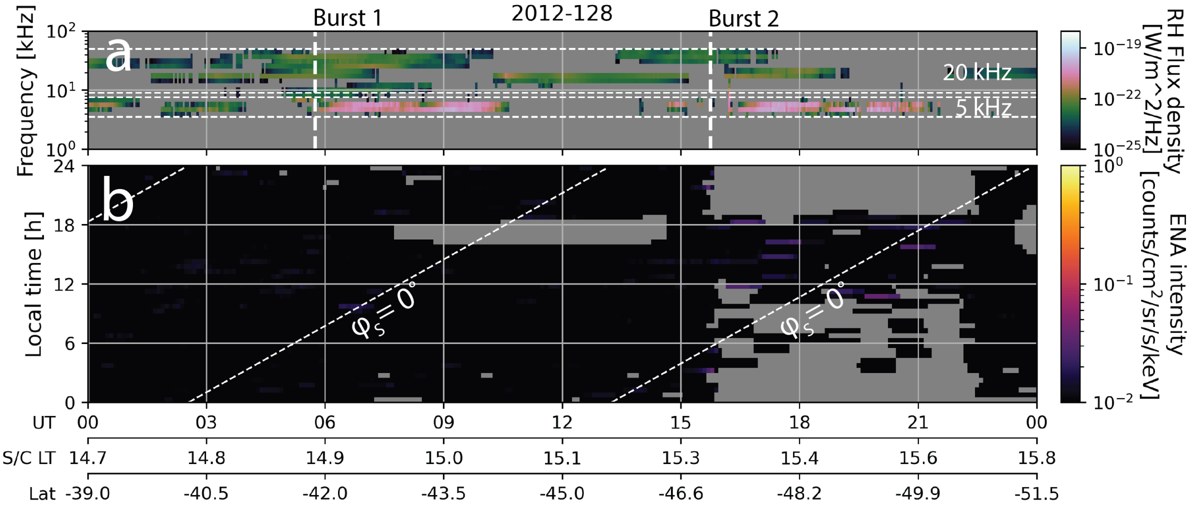

Figure 5: NB emission in the RH flux density (5a) and ENA keogram (5b) from 2013-128. Vertical lines in 5a mark the approximate start times of the two NB bursts, ten hours apart (clearest in the 5 kHz band here). Dashed diagonal lines in 5b indicate the local time direction of the rotating magnetic perturbation field dipole associated with Saturn's southern PPO system.

4 Summary

We have presented a pair of case studies showing how equatorial projections of Saturn's ENA emission intensity can be used to test the commonly observed correspondence with bursts of narrowband radio (NB) emission. The first case shows that the NB is enhanced in bursts as rotating regions of ENA emission pass through the dusk-midnight sector every near-planetary rotation. **Quantifying a correlation metric for this comparison is sensitive, though, to the radial distance range over which the projected ENA emission is counted.** When considering the *outer* (10-20 R_S) and *inner* (5-10 R_S) magnetospheric ENA emission separately, the local time of peak ENA-NB correlation shifts to later local times for inner ENA emission, a result of the spiral-like ENA morphology that develops following large-scale injections of energetic plasma that drift around and in towards the planet in time. While the inner magnetospheric correlation in the dusk sector is more intuitive considering other evidence (e.g., in situ detected injection signatures, conditions for production mechanisms), there is ambiguity in co-locating the potential source region of the narrowband emission with ENA emission structure.

The 5 kHz NB emission is more strongly correlated with the 24-55 keV ENA emission - when present - than the 20 kHz, likely because the 5 kHz intensity is higher at these spacecraft distances. Note that the generally more intense Z-mode proportion of the NB emissions do not reach beyond $\sim$5 R_S due to plasma and electron frequency dependencies, and beyond this the NB emissions mostly propagate in the O-mode (Ye et al., 2010; Menietti et al., 2016, 2019). The 5 kHz and 20 kHz emissions have different source regions and follow different ray paths (e.g. magnetopause reflections and plasma torus trapping), which could contribute to a weaker 20 kHz intensity observed at the spacecraft (e.g., Ye et al., 2009; Wang et al., 2010; Wu et al., 2021, 2022a). The correlation we're seeing is therefore likely related mostly to the L-O mode NB emissions detected outside $\sim$5 R_S, and a different relationship may exist for the stronger Z-mode emissions within the inner magnetosphere.

Lastly, there are times when the bursts of NB emission are clearly present but the ENA emission is almost entirely absent, despite comparable orbit positions. This could still be due to a combination of viewing effects , but it is also likely that the conditions for plasma radio wave production at the inner edge of the plasma torus are not *only* dependent on the global-scale injections visible in the ENA imagery at these energy ranges (see also Kinrade et al. (2020)). Thomsen et al. (2015) described a plasmapause-like boundary whereby large-scale injections 'prime' the inner magnetosphere with hot-cold plasma gradients and subsequent promotion of interchange instabilities that could feasibly be long-lasting.

We plan to follow up this case study with a statistical analysis of a collection of event comparisons, encapsulating the NB event lists of Wu et al. (2021), and the multiple species-energy ranges of the INCA instrument. This study will also examine rotational modulation effects in the frame of the PPO systems, which may tell us about the plasma sheet conditions possibly affecting the ENA and NB emissions.

5 Acknowledgements

The INCA ENA projections are accessible on the Lancaster University data repository and may be referenced using the dedicated DOI number (`https://doi.org/10.17635/lancaster/researchdata/384`). INCA, UVIS and RPWS data are available on NASA's Planetary Data System (PDS) (`https://pds.jpl.nasa.gov/`), and we thank the Cassini MIMI/INCA, UVIS and RPWS instrument teams. PPO phase data (2004-2017) were obtained from the University of Leicester Research Archive (`http://hdl.handle.net/2381/42436`), with our thanks to Gabby Provan for their production. Cross correlations were performed using the Pandas package 'corr' function (`https://pandas.pydata.org/docs/reference/api/pandas.DataFrame.corr.html`. Kinrade and Badman were supported by STFC grant ST/V000748/1. The Cassini/RPWS/HFR Kronos collection (`https://lesia.obspm.fr/kronos/data/skr/`) has been produced by B. Cecconi, L. Lamy, P. Zarka & P. Schippers, from the Observatoire de Paris/LESIA Cassini-RPWS team, with the support of CNRS and CNES. Jackman's, Louis', and O'Dwyer's work at the Dublin Institute for Advanced Studies was funded by Science Foundation Ireland Grant 18/FRL/6199. The authors thank Siyuan Wu for useful discussion about this work at the *PRE IX* meeting in Dublin.

References

Azari A. R., et al., 2018, Interchange Injections at Saturn: Statistical Survey of Energetic H+Sudden Flux Intensifications, *Journal of Geophysical Research: Space Physics*, *123, 4692*

Bader A., Kinrade J., Badman S. V. B., Paranicas C., Constable D. A., Mitchell D. G., 2021, A complete dataset of equatorial projections of Saturn's energetic neutral atom emissions observed by Cassini-INCA, *Journal of Geophysical Research: Space Physics*, *126, e2020JA028908*

Bradley T. J., Cowley S. W. H., Bunce E. J., Smith A. W., Jackman C. M., Provan G., 2018, Planetary Period Modulation of Reconnection Bursts in Saturn's Magnetotail, *Journal of Geophysical Research: Space Physics*, *123, 9476*

Brandt P. C., Paranicas C. P., Carbary J. F., Mitchell D. G., Mauk B. H., Krimigis S. M., 2008, Understanding the global evolution of Saturn's ring current, *Geophysical Research Letters*, *35, 1*

Carbary J. F., Mitchell D. G., 2014, Keogram analysis of ENA images at Saturn, *Journal of Geophysical Research: Space Physics*, *119, 1771*

Carbary J. F., Mitchell D. G., Brandt P., Paranicas C., Krimigis S. M., 2008a, ENA periodicities at Saturn, *Geophysical Research Letters*, *35, 1*

Carbary J. F., Mitchell D. G., Brandt P., Roelof E. C., Krimigis S. M., 2008b, Statistical morphology of ENA emissions at Saturn, *Journal of Geophysical Research: Space Physics*, *113, 1*

Gurnett D. A., 2004, The Cassini Radio and Plasma Wave Investigation, *Space Science Reviews*, *114, 395*

Gurnett D. A., Kurth W. S., Scarf F. L., 1981, Narrowband electromagnetic emissions from Saturn's magnetosphere, *Nature*, *292, 733*

Hill T. W., et al., 2008, Plasmoids in Saturn's magnetotail, *Journal of Geophysical Research: Space Physics*, *113, 1*

Kinrade J., et al., 2020, Tracking Counterpart Signatures in Saturn's Auroras and ENA Imagery During Large-Scale Plasma Injection Events, *Journal of Geophysical Research: Space Physics*, *125, e2019JA027542*

Kinrade J., et al., 2021, The Statistical Morphology of Saturn's Equatorial Energetic Neutral Atom Emission, *Geophysical Research Letters*, *48*

Krimigis S. M., et al., 2004, Magnetosphere Imaging Instrument (MIMI) on the Cassini mission to Saturn/Titan, *Space Science Reviews*, *114, 233*

Lamy L., 2017, The Saturnian Kilometric Radiation before the Cassini Grand Finale, *in Proceedings of the 8th International Workshop on Planetary, Solar and Heliospheric Radio Emissions (PRE VIII)*, Seggauberg, Austria, `http://arxiv.org/abs/1709.07693`

Lamy L., Zarka P., Cecconi B., Prangé R., Kurth W. S., Gurnett D. A., 2008, Saturn kilometric radiation: Average and statistical properties, *Journal of Geophysical Research: Space Physics, 113, 1*

Lamy L., Cecconi B., Prangé R., Zarka P., Nichols J. D., Clarke J. T., 2009, An auroral oval at the footprint of Saturns kilometric radio sources, colocated with the UV aurorae, *Journal of Geophysical Research: Space Physics, 114, 1*

Louarn P., et al., 2007, Observation of similar radio signatures at Saturn and Jupiter: Implications for the magnetospheric dynamics, *Geophysical Research Letters, 34, 2*

Menietti J. D., Ye S.-Y., Yoon P. H., Santolik O., Rymer A. M., Gurnett D. A., Coates A. J., 2009, Analysis of narrowband emission observed in the Saturn magnetosphere, *Journal of Geophysical Research: Space Physics, 114*

Menietti J. D., Yoon P. H., Písa D., Ye S.-Y., Santolík O., Arridge C. S., Gurnett D. A., Coates A. J., 2016, Source region and growth analysis of narrowband Z-mode emission at Saturn, *Journal of Geophysical Research: Space Physics, 121*

Menietti J. D., Yoon P. H., Pisa D., Averkamp T. F., Sulaiman A. H., Kurth W. S., Santolík O., Arridge C. S., 2019, The Role of Intense Upper Hybrid Resonance Emissions in the Generation of Saturn Narrowband Emission, *Journal of Geophysical Research: Space Physics, 124, 5709*

Mitchell D. G., et al., 2009, Recurrent energization of plasma in the midnight-to-dawn quadrant of Saturn's magnetosphere, and its relationship to auroral UV and radio emissions, *Planetary and Space Science, 57, 1732*

Mitchell D. G., et al., 2015, in eds Keiling A., Jackman C. M., Delamere P. A., , , Magnetotails in the Solar System. John Wiley and Sons, Inc., Hoboken, NJ, doi:10.1002/9781118842324.ch19, `http://onlinelibrary.wiley.com/doi/10.1002/9781118842324.ch19/summary`

Palmaerts B., Yao Z. H., Sergis N., Guo R. L., Grodent D., Dialynas K., Gérard J. C., Mitchell D. G., 2020, A Long-Lasting Auroral Spiral Rotating Around Saturn's Pole, *Geophysical Research Letters, 47, 1*

Paranicas C., Mitchell D. G., Roelof E. C., Brandt P. C., Williams D. J., Krimigis S. M., Mauk B. H., 2005, Periodic intensity variations in global ENA images of Saturn, *Geophysical Research Letters, 32, 1*

Provan G., 2018, PPO Phases 2004-2017, `https://hdl.handle.net/2381/42436`

Smith H. T., Richardson J. D., 2021, The 3D Structure of Saturn Magnetospheric Neutral Tori Produced by the Enceladus Plumes, *Journal of Geophysical Research: Space Physics, 126, 1*

Thomsen M. F., et al., 2010, Survey of ion plasma parameters in Saturn's magnetosphere, *Journal of Geophysical Research: Space Physics, 115, 1*

Thomsen M. F., Mitchell D. G., Jia X., Jackman C. M., Hospodarsky G., Coates A. J., 2015, Plasmapause formation at Saturn, *Journal of Geophysical Research: Space Physics*, *120, 2571*

Wang Z., Gurnett D. A., Fischer G., Ye S. Y., Kurth W. S., Mitchell D. G., Leisner J. S., Russell C. T., 2010, Cassini observations of narrowband radio emissions in Saturn's magnetosphere, *Journal of Geophysical Research: Space Physics*, *115, 1*

Wing S., Brandt P. C., Mitchell D. G., Johnson J. R., Kurth W. S., Menietti J. D., 2020, Periodic Narrowband Radio Wave Emissions and Inward Plasma Transport at Saturn's Magnetosphere, *The Astronomical Journal*, *159, 249*

Wu S., Ye S., Fischer G., Wang J., Long M., Menietti J. D., Cecconi B., Kurth W. S., 2021, Statistical Study on Spatial Distribution and Polarization of Saturn Narrowband Emissions, *The Astrophysical Journal*, *918, 64*

Wu S. Y., Ye S. Y., Fischer G., Jackman C. M., Wang J., Menietti J. D., Cecconi B., Long M. Y., 2022a, Reflection and Refraction of the L-O Mode 5 kHz Saturn Narrowband Emission by the Magnetosheath, *Geophysical Research Letters*, *49, 1*

Wu S. Y., et al., 2022b, Saturn Anomalous Myriametric Radiation, a New Type of Saturn Radio Emission Revealed by Cassini, *Geophysical Research Letters*, *49*

Ye S. Y., et al., 2009, Source locations of narrowband radio emissions detected at Saturn, *Journal of Geophysical Research: Space Physics*, *114, 1*

Ye S. Y., Menietti J. D., Fischer G., Wang Z., Cecconi B., Gurnett D. A., Kurth W. S., 2010, Z mode waves as the source of saturn narrowband radio emissions, *Journal of Geophysical Research: Space Physics*, *115, 1*

Ye S.-Y., Fischer G., Menietti J. D., Wang Z., Gurnett D. A., Kurth W. S., 2011, An Overview of Saturn Narrowband Radio Emissions Observed by Cassini RPWS (invited), *in Planetary Radio Emissions VII, Proceedings of the 7th International Workshop, eds Rucker H. O., Kurth W. S., Louarn P., Fischer G., , Vol. VII*, Austrian Academy of Sciences Press, Graz, Austria, pp 99–114, doi:10.1553/pre7s99, `https://ui.adsabs.harvard.edu/abs/2011pre7.conf...99Y/abstract`